Progress in Photovoltaics: Research and Applications

WILEY

PROGRESS IN PHOTOVOLTAICS

RESEARCH ARTICLE

Novel Nano-Pyramid/Polish Hybrid Morphology Designed for High-Efficiency Passivated Contact Solar Cells

Baochen Liao[1] | Sheng Ma[2] | Reuben J. Yeo[3] | Xinyuan Wu[4] | Shuai Zou[5] | Xiaodong Su[5] | Wenzhong Shen[2] | Guoqiang Xing[6] | Bram Hoex[4]

[1]School of Microelectronics and Integrated Circuits (Jiangsu Key Laboratory of Semi. Dev. & IC Design, Package and Test), Nantong University, Jiangsu, China | [2]Institute of Solar Energy, Shanghai Jiao Tong University, Shanghai, China | [3]Agency for Science, Technology and Research (A*STAR), Institute of Materials Research and Engineering (IMRE), Singapore, Singapore | [4]School of Photovoltaic and Renewable Energy Engineering, University of New South Wales, Sydney, Australia | [5]School of Physical Science and Technology, and Jiangsu Key Laboratory of Thin Films, Soochow University, Jiangsu, China | [6]Tongwei Solar Co., Ltd., Meishan, Sichuan, China

Correspondence: Baochen Liao (liaobaochen@ntu.edu.cn) | Sheng Ma (mas123@sjtu.edu.cn) | Wenzhong Shen (wzshen@sjtu.edu.cn) | Guoqiang Xing (xinggq01@tongwei.com)

Received: 6 March 2025 | **Revised:** 19 May 2025 | **Accepted:** 29 May 2025

Funding: This work was supported by the funding support of the Jiangsu Specially Appointed Professor grant (Grant No. 06210061007), the Major State Basic Research Development Program of China (Grant No. 2022YFB4200101), Inner Mongolia Science and Technology Project (Grant No. 2022JBGS0036), Yibin Science and Technology Project and the Research Funding for High-level Talents of Nantong University (No. 03083035).

Keywords: additive | nano-pyramid | nano-pyramid/polish hybrid morphology | secondary textured | TOPCon

ABSTRACT

In photovoltaic applications, the rear surface morphology of tunnel oxide passivated contact (TOPCon) solar cells plays a critical role in their performance. However, traditional textured and polished surface morphologies both have limitations. This study introduces a hybrid nano-pyramid/polish morphology, combining a nano-pyramid structure on a polished surface. This new design aims to capitalize on the advantages of both textured and polished surfaces, achieving an optimal balance for TOPCon performance. The balance is achieved through an additional chemical solution treatment process. When applied to TOPCon solar cells, the hybrid structure outperforms both secondary-textured and polished morphologies in terms of optical absorption, passivation, and contact performance. The nano-pyramid/polish hybrid achieves a superior balance between light trapping, passivation, and contact quality. Furthermore, the study investigates the impact of rear surface morphology on film blistering, revealing that rougher surfaces are less prone to blistering. This is likely due to more favorable stress distribution in the SiO_x/poly-Si stack, enhancing mechanical stability. These findings demonstrate the compatibility of the hybrid nano-pyramid/polish morphology with TOPCon solar cells, offering a promising pathway to enhance efficiency. The insights gained may also benefit the development of other high-performance solar cell technologies, such as heterojunction (HJT) and silicon/perovskite tandem solar cells, advancing industrial photovoltaic applications.

1 | Introduction

Passivation contact technology has emerged as a highly effective method for enhancing the efficiency of silicon solar cells [1, 2]. This technology mitigates the recombination losses typically associated with metal–semiconductor contacts, thereby enabling significant improvements in the overall efficiency of commercial solar cells [3, 4]. The exceptional surface and chemical passivation effects in tunnel oxide passivated contact (TOPCon) cells are attributed to the incorporation of a heavily doped polysilicon (poly-Si) layer and an ultra-thin tunnel SiO_x layer [5]. Building on the concept of carrier selectivity,

Schmidt et al. proposed a theoretical limit efficiency of 28.7% for TOPCon cells [4]. Additionally, existing passivated emitter and rear contact (PERC) solar cell production lines can easily be upgraded to TOPCon production lines. Consequently, n-type TOPCon cells are widely regarded as one of the most promising next-generation high-efficiency crystalline silicon cell technologies [6, 7]. Since 2022, n-TOPCon solar cells have become a preferred technology among mainstream industrial manufacturers, achieving a remarkably low recombination current density (J_0) of less than 3 fA/cm^2 and a low contact resistivity (ρ_c) of less than 10 mΩ·cm^2 [8, 9]. The efficiency of large-area TOPCon solar cells designed for mass production has also seen continuous improvements. Recent reports indicate that the highest efficiency achieved for such cells now exceeds 25% [10, 11]. This consistent enhancement in efficiency underscores the significant potential of TOPCon technology to dominate future solar cell markets and drive the next wave of advancements in photovoltaic performance.

Given that the SiO_x/phosphorus (P) doped n^+ poly-Si structure is deposited on the rear surface of TOPCon cells, the morphology of the rear surface has a significant impact on the overall performance of the cells [12]. For example, a textured morphology on the rear surface comes with several drawbacks. Firstly, previous studies [13–16] have indicated that forming high-quality passivating contact structures on textured surfaces is challenging, which inevitably results in increased J_0 values compared to planar surfaces. This difficulty arises because the pyramidal morphology exposes a substantial amount of surface area with a Si (111) crystal orientation, resulting in the formation of a SiO_x/Si (111) interface where the density of defects is approximately 10 times higher than at the SiO_x/Si (100) interface [17, 18]. Secondly, the textured surface causes inconsistencies in the thickness of the ultra-thin SiO_x layer at the vertices, edges, and valleys of the pyramids, which makes it easier for cracks to form during subsequent high-temperature annealing steps [19, 20]. Thirdly, the antireflective nature of the pyramidal surface allows more light to enter the n^+ poly-Si layer, leading to increased optical losses [21, 22]. Therefore, to enhance passivation characteristics and optical absorption, a smoother and higher reflectivity polished surface emerges as an effective optimization direction. This approach aims to mitigate the aforementioned challenges associated with the textured surface, thereby improving the overall performance of TOPCon cells.

On the other hand, the optimization of metal contact on TOPCon cells requires an approach that contrasts with the need for passivation contact performance. Pyramid faces are more conducive to forming good electrical contacts, thereby reducing contact resistance [23–26]. This improvement is likely related to the formation of silver crystallites [12, 26] and the mode of carrier transport. On the surface of the pyramids, the doping concentration at the vertices is higher than at the valleys, leading to higher electron concentrations at these points, which facilitates the conversion of silver ions into silver crystallites [27]. Additionally, the vertices of pyramidal surfaces are more likely to achieve direct contact during carrier transport, which is crucial for maintaining low contact resistance. Moreover, a rougher rear surface morphology increases the contact area between the rear surface and the metal during the metallization process, which is beneficial for reducing contact resistance. Therefore, designing the rear surface morphology to balance optimal electrical performance and passivation quality is a crucial area of research.

In this paper, we introduce a nano-pyramid/polish hybrid rear surface morphology design for TOPCon solar cells aimed at achieving optimal cell performance across multiple metrics. This novel morphology is engineered by precisely controlling the corrosion rate of the rear surface silicon using a tailored recipe of chemical solution treatments, resulting in a nano-pyramid structure on a polished surface. The effectiveness of this morphology was evaluated through comprehensive optical, passivation, and contact performance tests. When compared to secondary-textured (two-step texturing with a slower reaction rate for the second step to improve light trapping) and polished morphologies, the proposed nano-pyramid/polish hybrid morphology design demonstrated superior electrical performance, achieving an ideal balance between light trapping, surface passivation, and contact quality. These findings underscore the compatibility of this morphology with TOPCon cells, presenting it as a transformative approach for enhancing cell efficiency. The insights gained from this study highlight the significant potential of this design for its application in other high-efficiency solar cell technologies, such as the rear surface of heterojunction technology (HJT) solar cell and the interface of silicon/perovskite tandem solar cells, paving the way for significant enhancements in industrial photovoltaic performance.

2 | Experimental Details

To evaluate the impact of different rear surface morphologies on the performance of TOPCon solar cells, industrial-scale cells were fabricated using Czochralski (Cz) n-type silicon wafers. These wafers feature M10 dimensions of 182 × 182 mm^2, a thickness of 150 ± 20 μm, and a resistivity range of 0.3–2.1 Ω·cm, aligning with current industrial standards for high-efficiency cell production.

Comprehensive characterization techniques were employed to assess the influence of rear morphologies on key performance metrics, including optical absorption, passivation quality, and contact performance.

2.1 | Methods for Obtaining Different Rear Surface Morphologies

To evaluate the performance of TOPCon solar cells with different rear morphologies, three distinct chemical solution treatments were applied to modify the cell rear surface. Figure 1b illustrated the specific formulation ratios and processing conditions for each chemical treatment. Flowchart showing the chemical solution treatments used to achieve the different rear surface morphologies was shown in Figure 1c. Details of the specific method of chemical solution treatment are as follows:

Step1: Raw silicon wafers for industrial use are typically treated with an alkaline solution combined with a

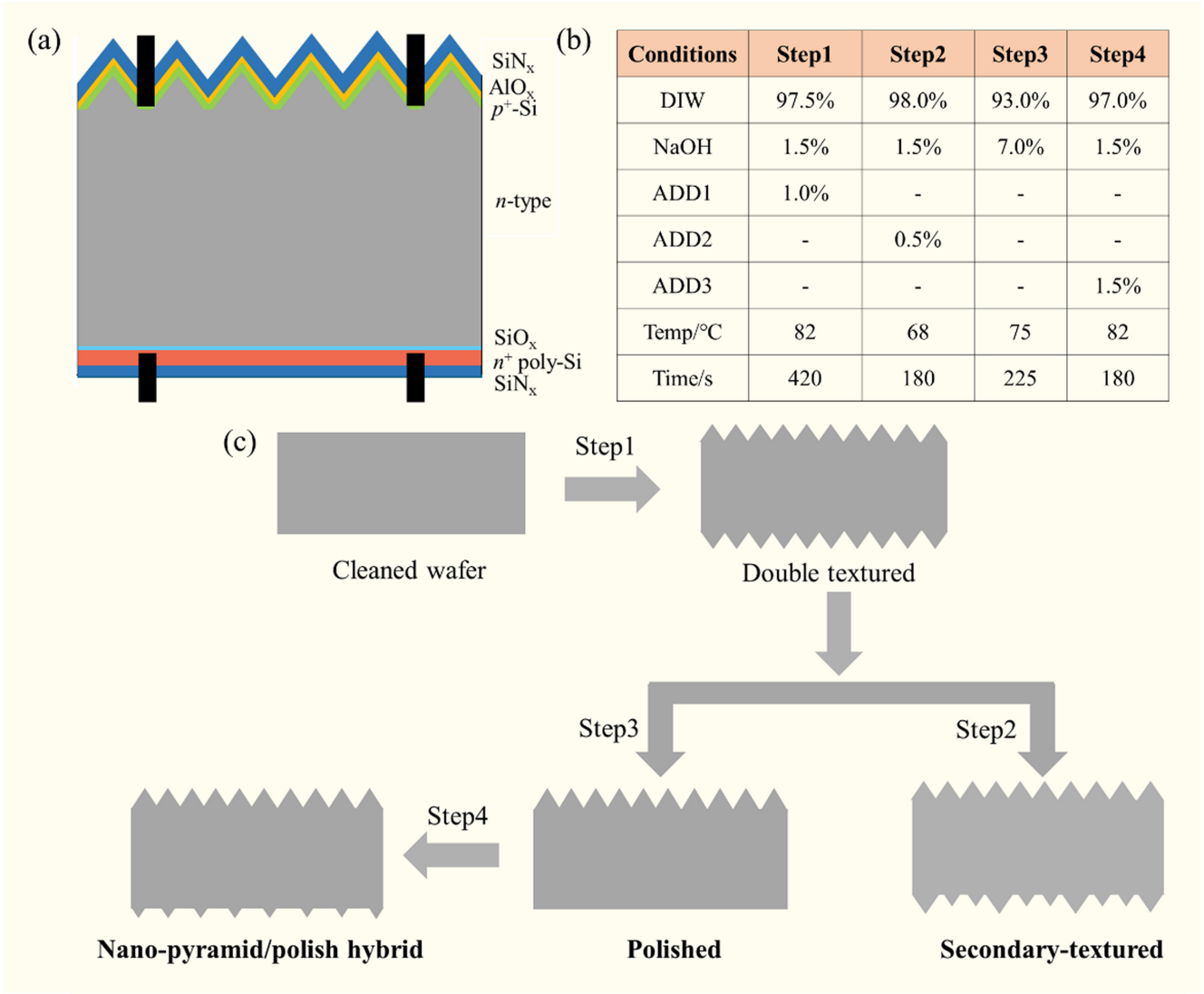

Conditions	Step1	Step2	Step3	Step4
DIW	97.5%	98.0%	93.0%	97.0%
NaOH	1.5%	1.5%	7.0%	1.5%
ADD1	1.0%	-	-	-
ADD2	-	0.5%	-	-
ADD3	-	-	-	1.5%
Temp/°C	82	68	75	82
Time/s	420	180	225	180

FIGURE 1 | (a) Schematic of an n-type TOPCon bifacial silicon solar cell with planar rear surface. (b) The specific formulation ratios and processing conditions for each chemical treatment. (c) Flowchart showing the chemical solution treatments used to achieve the different rear surface morphologies.

specialized additive (SunFonergy, MQT-810A) to create a double-textured morphology on both sides of the wafer.

Step2: Secondary-textured morphology: This morphology builds upon the pyramid texture by applying an alkaline solution combined with a specialized additive (Topone Tech, TB186) that creates smaller pyramids in certain areas of the surface.

Step3: Polished morphology: This structure is achieved by using an alkaline solution to smooth out the pyramid texture, resulting in a flat surface.

Step4: Nano-pyramid/polish hybrid morphology: Starting from the polished structure, a further chemical treatment is applied to form small pyramids on the surface, creating a nano-pyramid pattern via a tailored additive (SunFonergy, MQT-709) to suppress hydroxyl reactivity in the presence of KOH etching.

2.2 | Fabrication of TOPCon Solar Cells

To investigate the effect of different rear morphologies on cell performance, the manufacturing process of TOPCon cells was carried out on the production line following the steps as shown in process in Figure 2a. The n-type wafers were initially subjected to saw-damage etching (SDE) using potassium hydroxide (KOH), followed by an alkaline texturing process on both sides, resulting in a pyramid structure approximately 2 μm in size. After cleaning, boron diffusion was carried out in a tube furnace with boron trichloride (BCl_3) as the dopant source to form a p^+ layer. Subsequently, an inline single-side etch (SSE) was performed to remove the wrap-around p^+ doping, and the different rear morphologies were obtained by different chemical solution treatments, as shown in Figure 1. The SiO_x and in situ phosphorus-doped amorphous silicon (a-Si) layers were deposited using a tube plasma-enhanced chemical vapor deposition (PECVD) system (*ZR5000, Leadmicro*).

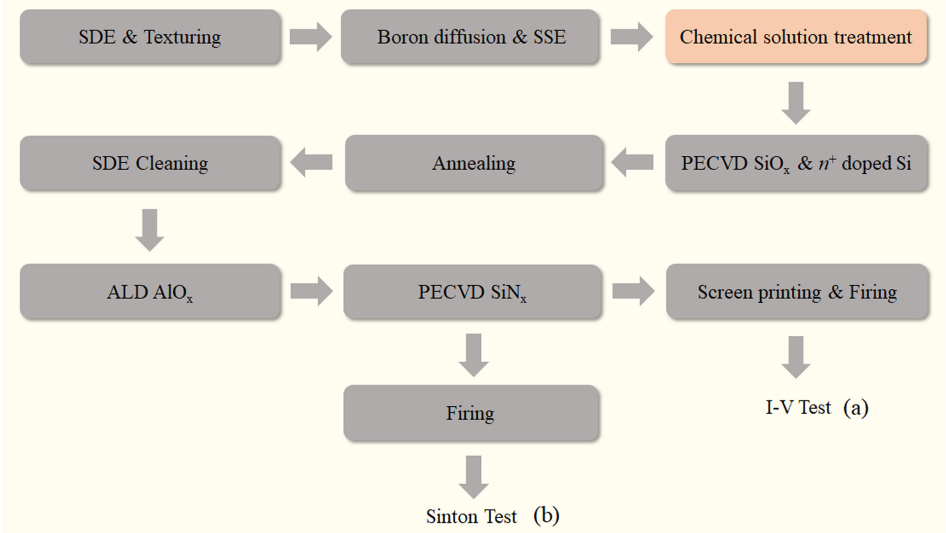

FIGURE 2 | Fabrication process flows for the TOPCon solar cells (a) and the lifetime samples (b).

The annealing process was carried out in a nitrogen (N_2) atmosphere (*XH10000A, Leadmicro*) at a temperature of 900°C for 45 min. After annealing, the edge wrap-around deposition of polycrystalline silicon was removed using a hot KOH solution. The front side was capped with a 3-nm layer of AlO_x using a tube atomic layer deposition (ALD) system (*KF15000P, Leadmicro*). Subsequently, both sides were coated with a 70-nm layer of SiN_x using a tube PECVD system (*ZR5000, Leadmicro*). Finally, the electrode patterns were fabricated by screen printing (*Softline-DL-SP, Maxwell*) using Ag-Al paste on the front side and Ag paste on the rear side, followed by an industrial belt-furnace fast-firing to form the metal contacts and activate hydrogen atoms.

2.3 | Characterization

To evaluate the surface passivation quality with different morphologies, samples were fabricated according to process as shown in Figure 2b. The preparation process was similar to that used for the cells, with the main difference being that after the SiN_x film layer was deposited, it underwent firing without screen printing. The effective minority carrier lifetime and J_0 were measured by a quasi-steady-state photoconductance method (*WCT-120, Sinton Instruments*) at an injection density of $1\times10^{16}\,cm^{-3}$ [28–30]. The surface morphologies of the samples were investigated by optical microscopy (*Leica DM 4000*), scanning electron microscopy (SEM, *Jeol JSM-7800F*), and atomic force microscopy (AFM, *Semilab Gemini 360*). Raman measurements, used for extracting the crystalline fractions and internal stresses, were conducted using a 325-nm excitation laser (*Renishaw, inVia Qontor*). The residual stress can be calculated using the following formula [31]:

$$\sigma = -435\,\Delta w(\mathrm{MPa})$$

where σ is the Raman shift offset relative to the standard Raman peak of c-Si ($520\,cm^{-1}$). Positive and negative σ indicate compressive and tensile stresses, respectively. A simulation was carried out to study the optical absorption differences of cells with different rear morphologies through the *Comsol Multiphysics* software. The contact resistivity (ρ_c) was measured by the transmission line method (*TLM, Ai-shine*). The electrical parameters of the cells were measured by *Halm 3600* under standard test conditions (AM 1.5 G spectrum, 25°C).

3 | Results and Discussion

3.1 | Surface Morphology

The morphology of the nano-pyramid/polish hybrid structure was thoroughly examined using SEM and AFM and compared with samples featuring polished and secondary-textured structures. Figure 3a–f presents top-view SEM and AFM images, revealing that the nano-pyramid/polish hybrid structure exhibits a morphology that lies between those of the polished and secondary-textured structures. Specifically, it features small, nonstandard pyramid structures on the polished surface, with significantly lower height and pyramid density compared to the secondary-textured structure. The 3D AFM images in Figure 3g–i further elucidate the morphological differences between the three surface textures. The analysis of the 3D AFM images reveals that the secondary-textured structure has a dense and uniformly distributed pyramid pattern, with pyramid heights primarily in the range of 1.3–1.7 μm. In contrast, the nano-pyramid/polish hybrid structure displays sparsely distributed pyramid structures with a height distribution within the range of 0.2–0.6 μm. This indicates a gradual reduction in surface roughness from the secondary-textured to the nano-pyramid/polish hybrid and polished structures. Moreover, the three different surface morphologies exhibited significant differences in reflectivity. The average reflectivity values for the secondary-textured, nano-pyramid/polish hybrid, and polished structures, as measured by spectroscopic ellipsometer over the wavelength range of 300–1200 nm, were 12%, 25%, and 40%, respectively. These results highlight the pronounced impact of the rear surface morphology on reflectivity, with important implications for optimizing the optical efficiency of solar cell designs.

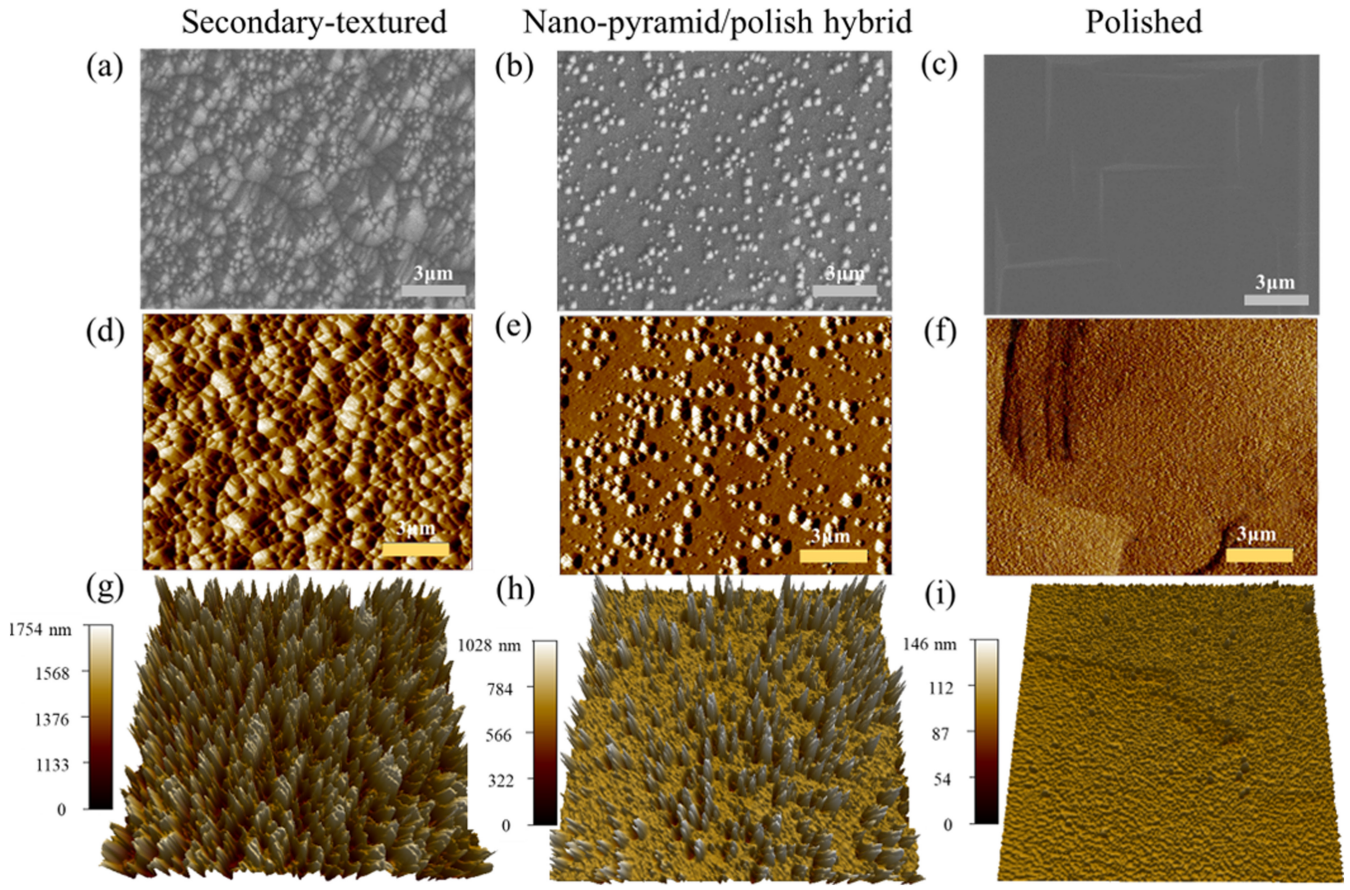

FIGURE 3 | Top-view SEM (a–c), 2D AFM (d–f), and 3D AFM (g–i) images for the secondary-textured, nano-pyramid/polish hybrid, and polished structures.

3.2 | Optical Performance

To study the influence of different rear surface morphologies on the optical performance of cells, we conducted three-dimensional simulations utilizing *Comsol Multiphysics* software to investigate the photovoltaic behavior of solar cells under omnidirectional incident angles. Schematics illustrating secondary-textured, nano-pyramid/polish hybrid, and polished structures are presented in Figure 4. The front surface morphology featured a normal pyramid structure. For the rear surface structure, from AFM measurements, the average heights of the pyramids in the secondary-textured and nano-pyramid/polish hybrid configurations were specified as 1.5 and 0.4 μm, respectively. To analyze the differences in light trapping mechanisms associated with different rear surface morphologies, we examined the electric field distributions in the TOPCon cells under illumination with wavelengths of 500 nm (Figure 4a) and 1000 nm (Figure 4b). At an incident light wavelength of 500 nm, the electric field distribution remained consistent across the cells despite the different rear surface structures (Figure 4a), indicating that there was minimal influence of the rear surface morphology on medium- and short-wave absorption. However, at an incident light wavelength of 1000 nm, a noticeable trend emerged. As the roughness of the rear surface decreased, the electric field intensity increased (Figure 4b), suggesting that a higher roughness impedes optical absorption. To substantiate this observation, we performed statistical analyses across various wavelength ranges, as presented in Figure 4c. Our findings revealed that the rear structure exerts no discernible effect on optical absorption within the medium to short wavelength range (300–900 nm). Conversely, in the long wavelength range (900–1200 nm), decreasing roughness correlates with enhanced optical absorption.

3.3 | Passivation and Contact Performance

To assess the influence of rear surface morphology on the cell's electrical performance, various characterization techniques were used to investigate passivation and contact characteristics for various rear surface morphologies. The samples used for passivation testing were semifinished cells prior to metallization process as seen in Figure 2b, while the samples used for contact testing were TOPCon cells with three rear morphologies. Figure 5a presents the measured J_0 and charge carrier lifetime using samples prepared as shown in Figure 2b. The results demonstrate that as the rear surface roughness decreased, J_0 decreased from 24.5 to 19.8 and 18.5 fA/cm^2, while the effective lifetime increased from 1772 to 2057 and 2071 μs, indicating a progressive increase in passivation quality. Regarding contact performance, the samples were evaluated using TLM, with the results shown in Figure 5b. As the rear surface roughness decreased, the contact resistivity increased from 0.74 to 0.86 mΩ·cm^2. This suggests that the nano-pyramid/polish hybrid structure did not significantly compromise the contact performance compared to the secondary-textured structure. However,

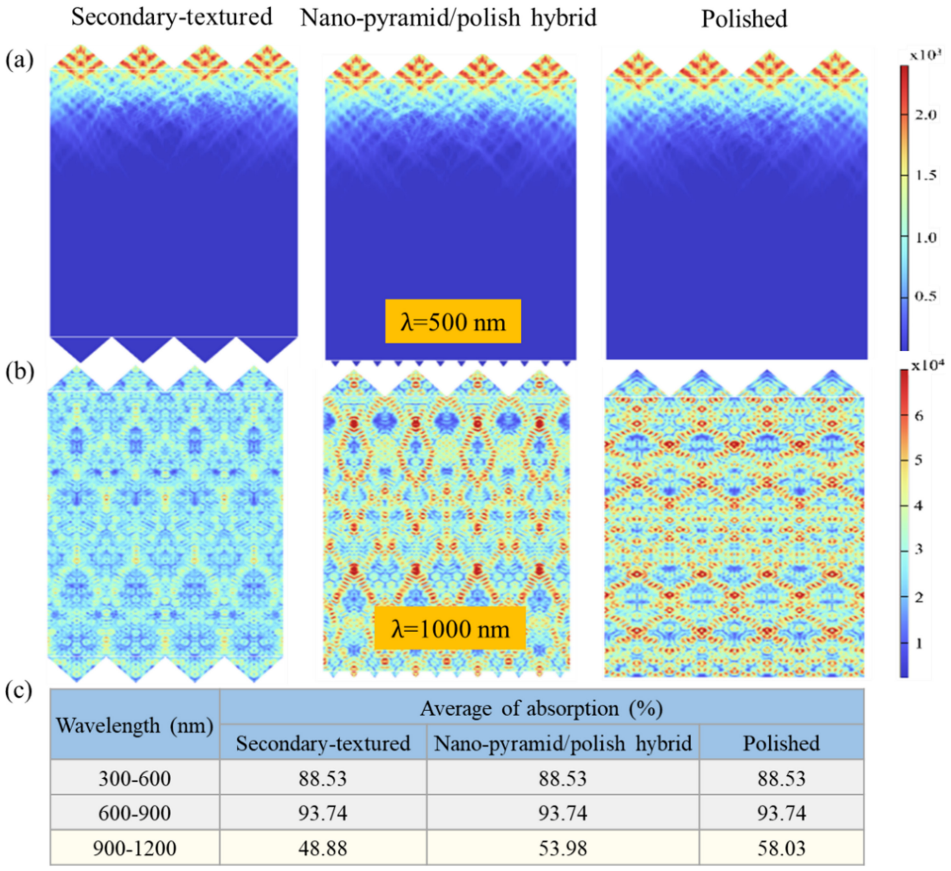

(c)

Wavelength (nm)	Average of absorption (%)		
	Secondary-textured	Nano-pyramid/polish hybrid	Polished
300-600	88.53	88.53	88.53
600-900	93.74	93.74	93.74
900-1200	48.88	53.98	58.03

FIGURE 4 | Electric field distributions for TOPCon solar cells with different rear structures at incident light wavelengths of 500 nm (a) and 1000 nm (b); (c) the corresponding average absorption for wavelengths in the ranges of 300–600, 600–900, and 900–1200 nm.

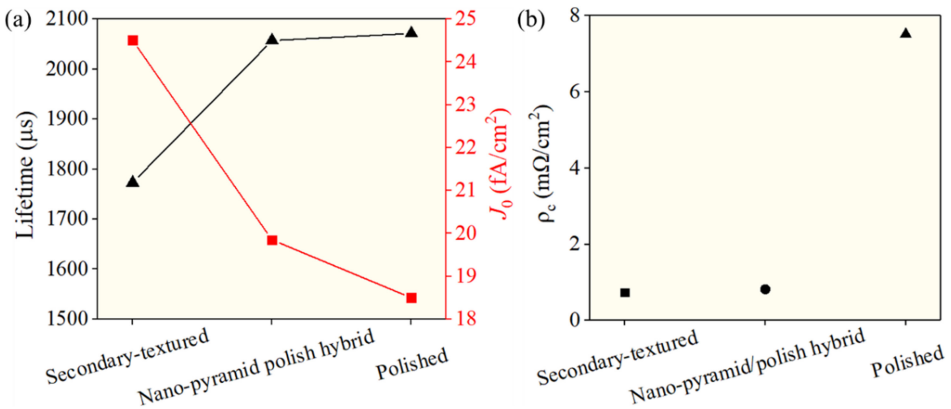

FIGURE 5 | (a) Measured J_0 and lifetime. (b) Contact resistivity (ρ_c) values of the samples were measured by the TLM.

with further reduction in roughness to a polished structure, the contact resistivity notably increased to 7.86 mΩ·cm^2, signifying a substantial decline in contact performance that could adversely affect the cell's electrical properties. This can be attributed to the reduction in contact area during rear metallization as roughness decreased. Considering both passivation and contact performance, it was determined that TOPCon solar cells achieved optimal performance with the nano-pyramid/polish hybrid structure. These research findings underscore the importance of implementing a nano-pyramid/polish hybrid structure to strike a balance between passivation quality and contact performance, ultimately leading to enhanced electrical characteristics. Such a strategic approach contributes significantly to the advancement of high-efficiency solar cell technologies.

3.4 | Blistering

It is well-known that PECVD in situ n^+ doped amorphous silicon (a-Si) is prone to blistering in the fabrication process of TOPCon solar cells, particularly after the annealing process. Blistering deteriorates the properties of the poly-Si/SiO_x interface due to the blistered areas being severely hampered, leading to the prevention of charge-carrier collection. In the worst case,

blisters may rupture from the surface of poly-Si, resulting in direct contact with the metal electrodes, and thus leading to high recombination loss [32]. To mitigate blistering, a very effective method is to adjust the internal stress in the films by modifying the surface morphology. Optical microscopy and SEM were employed to examine the surface characteristics of the samples with varying rear surface morphologies after annealing, as depicted in Figure 6a. Analysis of the images revealed that both the secondary-textured and nano-pyramid/polish hybrid structures did not exhibit any signs of blistering. Conversely, as the surface roughness decreased (as seen in the polished structure), irregularly sized bubbles began to appear, indicating potential cracking or peeling of the poly-Si film from the silicon substrate. These observations suggest that reduced surface roughness increases the likelihood of film blistering, which aligns with findings from previous studies. It is well-known that when a silicon film has a lattice mismatch with the silicon substrate, residual stress is likely to develop at their interface, potentially leading to film delamination. Raman spectroscopy studies were conducted to investigate the microstructural details and elucidate the blistering behavior of P-doped poly-Si films on different rear surface morphologies. When the material is under strain, its Raman characteristic peak will be shifted or deformed compared to that of the pristine state [33]; therefore, in this work, we extracted the values of residual stresses from the shifts in the Raman peak. Compared to the characteristic Si Raman peak located at 520 cm^{-1}, the peaks of P-doped poly-Si on different rear surface morphologies were gradually shifted towards higher frequency, as depicted in Figure 6b, thus verifying the presence of compressive stresses in the poly-Si films. For secondary-textured and nano-pyramid/polish hybrid structures, relatively lower compressive stresses of 31.4 and 32.6 MPa were achieved, whereas a much larger compressive stress of 509.2 MPa was determined for the polished structure as seen in Figure 6c. When the poly-Si film is subjected to compressive stress, the spacing between the adjacent atoms decreases. As the residual stress surpasses the fracture strength of the material, some of this residual stress is released through blister formation [34]. Therefore, increasing the roughness of the rear surface is beneficial for suppressing the blistering of the poly-Si film. In summary, the polished morphology is more susceptible to film blistering compared to the other two profiles, posing a risk of degradation in the passivation contact performance of cells with this morphology.

3.5 | Cell Performance

In the final evaluation of different rear surface morphologies at the device level, TOPCon solar cells were fabricated using 600 pieces of M10 wafers, with passivation layers incorporating secondary-textured, nano-pyramid/polish hybrid, and polished morphologies. The cells were fabricated in an industrial TOPCon

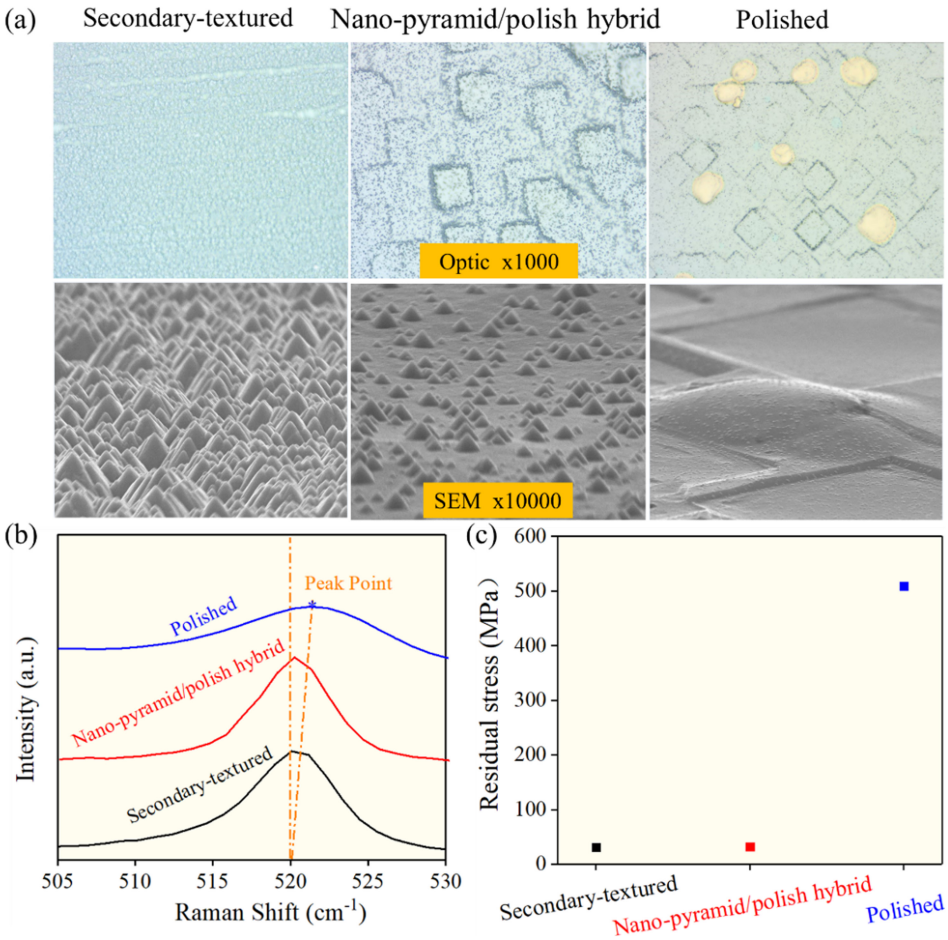

FIGURE 6 | (a) Optical and SEM images of P-doped poly-Si films on different rear surface morphologies after annealing. (b) Raman spectra under the range of 505–530 cm^{-1}. (c) Residual stresses extracted from the Raman Si peak intensities and shifts.

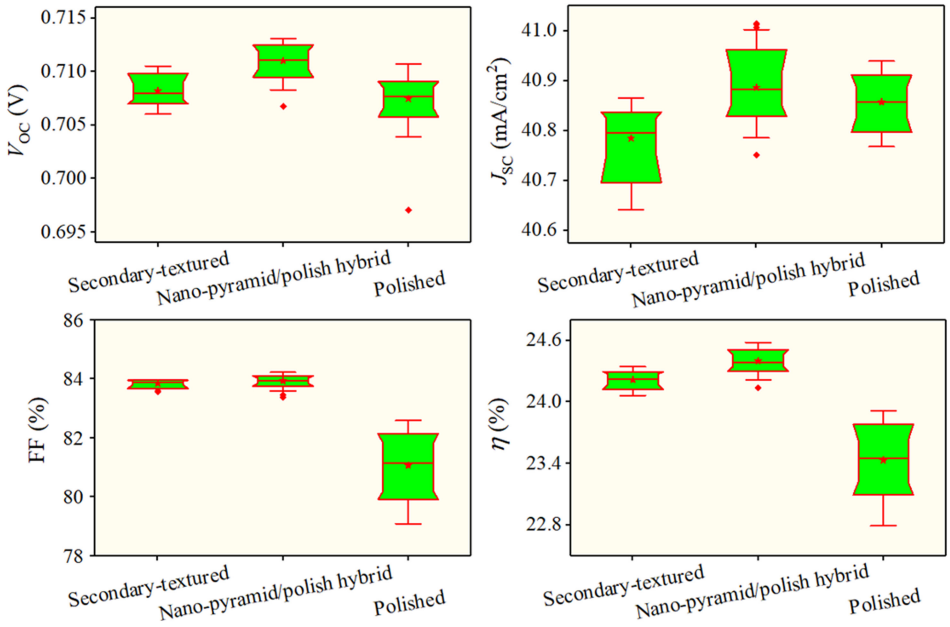

FIGURE 7 | Measured *J-V* parameters of TOPCon solar cells with different rear surface morphologies fabricated on a TOPCon cell production line using M10 wafers.

production line, ensuring consistency with industrial manufacturing standards. The electrical parameter results measured on the fabricated TOPCon cells are presented in Figure 7. Although the cells with polished morphology have a higher average short circuit current density (J_{SC}) value than the secondary-textured cells, they have a much lower fill factor (FF). This is consistent with their optical performance and contact performance as discussed previously. These results reveal the limitations of the fully polished and fully textured morphologies. In contrast, the cells with the nano-pyramid/polish hybrid morphology inherit the advantages of both the textured and polished surfaces. The high J_{SC} obtained for the hybrid morphology cells was comparable with that of the polished surface, whereas the high FF was comparable with that of the secondary-textured surface. In terms of the open circuit voltage (V_{OC}), the cells with nano-pyramid/polish hybrid morphology achieved the highest average V_{OC} of 711.2 mV, and not the cells with polished surface, unlike the lifetime measurement results. This could be due to the much lower FF of the cells with the polished morphology. Notably, the cell's conversion efficiency (η) was maximized with the nano-pyramid/polish hybrid rear surface structure, achieving an impressive average η of 24.4%. This represents an enhancement of 0.18% and 0.96% compared to the secondary-textured and polished morphologies, respectively. The improved cell performance is attributed to the nano-pyramid/polish hybrid design in attaining an overall beneficial compromise between passivation quality and contact performance, leading to the advancement of TOPCon cell efficiency. This optimal configuration underscores the advantage of having a moderate rear surface roughness, which effectively balances light trapping and electrical contact reliability.

4 | Conclusions

In this paper, we introduce a novel nano-pyramid/polish hybrid morphology achieved by inducing a nano-pyramid structure on a polished surface through an additional chemical solution treatment. This approach addresses the limitations of secondary-textured and polished morphologies by optimizing the balance between optical absorption, passivation, and contact performance. Comparative analyses revealed that while the polished structure excelled in optical absorption and passivation, it exhibited poor contact performance and was prone to surface film blistering. The proposed nano-pyramid/polish hybrid morphology offers a compelling compromise, demonstrating improved contact performance while maintaining competitive optical and passivation characteristics. To validate its practical applicability, we fabricated TOPCon solar cells with these three rear morphologies on an industrial production line. The cells with the proposed nano-pyramid/polish hybrid morphology achieved the highest conversion efficiency, surpassing that of secondary-textured and polished morphologies by 0.18% and 0.96%, respectively. These results highlight the potential of the nano-pyramid/polish hybrid morphology as a transformative design for achieving superior electrical performance in TOPCon cells. Furthermore, the nano-pyramid/polish hybrid morphology can also be useful in the further advancement of other modern, high-efficiency photovoltaic technologies where the surface or interface morphology would be an important consideration—for example, in the rear surface design of HJT or in the interface design of Si/perovskite tandem cells. By adopting such nano-pyramid/polish hybrid designs, a strategic balance between optical and electrical optimization can be achieved, paving the way for further improvements in photovoltaic applications.

Author Contributions

Baochen Liao: writing – original draft, methodology, investigation, formal analysis, funding acquisition, supervision, conceptualization. **Sheng Ma:** writing – original draft, data curation, investigation, formal analysis. **Reuben J. Yeo:** writing – review and editing, methodology. **Xinyuan Wu:** methodology, data curation. **Shuai Zou:** writing – review and editing, methodology. **Xiaodong Su:** conceptualization.

Wenzhong Shen: supervision, funding acquisition, conceptualization. **Guoqiang Xing:** supervision, methodology, conceptualization. **Bram Hoex:** supervision, methodology, conceptualization.

Acknowledgments

The authors acknowledge the support from the industrial partners. This work was supported by the funding support of the Jiangsu Specially-Appointed Professor grant (Grant No. 06210061007), the Major State Basic Research Development Program of China (Grant No. 2022YFB4200101), Inner Mongolia Science and Technology Project (Grant No. 2022JBGS0036), Yibin Science and Technology Project and the Research Funding for High-level Talents of Nantong University (No. 03083035).

Data Availability Statement

The data that support the findings of this study are available from the corresponding author upon reasonable request.

References

1. F. Feldmann, M. Bivour, C. Reichel, M. Hermle, and S. W. Glunz, "Passivated Rear Contacts for High-Efficiency n-Type Si Solar Cells Providing High Interface Passivation Quality and Excellent Transport Characteristics," *Solar Energy Materials and Solar Cells* 120 (2014): 270–274, https://doi.org/10.1016/j.solmat.2013.09.017.

2. F. Feldmann, M. Bivour, C. Reichel, H. Steinkemper, M. Hermle, and S. W. Glunz, "Tunnel Oxide Passivated Contacts as an Alternative to Partial Rear Contacts," *Solar Energy Materials and Solar Cells* 131 (2014): 46–50, https://doi.org/10.1016/j.solmat.2014.06.015.

3. J. Melskens, B. W. H. van de Loo, B. Macco, L. E. Black, S. Smit, and W. M. M. Kessels, "Passivating Contacts for Crystalline Silicon Solar Cells: From Concepts and Materials to Prospects," *IEEE Journal of Photovoltaics* 8, no. 2 (2018): 373–388.

4. J. Schmidt, R. Peibst, and R. Brendel, "Surface Passivation of Crystalline Silicon Solar Cells: Present and Future," *Solar Energy Materials and Solar Cells* 187 (2018): 39–54, https://doi.org/10.1016/j.solmat.2018.06.047.

5. A. G. Aberle, S. W. Glunz, A. W. Stephens, and M. A. Green, "High-Efficiency Silicon Solar Cell: Si/SiO_2 Interface Parameters and Their Impact on Device Performance," *Progress in Photovoltaics: Research and Applications* 2 (1994): 265–273.

6. T. G. Allen, J. Bullock, X. B. Yang, A. Javey, and S. D. Wolf, "Passivating Contacts for Crystalline Silicon Solar Cells," *Nature Energy* 4, no. 11 (2019): 914–928.

7. Y. Zhou, K. Tao, A. Liu, et al., "Screen-Printed n-Type Industry Solar Cells With Tunnel Oxide Passivated Contact Doped by Phosphorus Diffusion," *Superlattices and Microstructures* 148 (2020): 106720, https://doi.org/10.1016/j.spmi.2020.106720.

8. J. Sheng, Z. Ma, W. Cai, et al., "Impact of Phosphorus Diffusion on n-Type Poly-Si Based Passivated Contact Silicon Solar Cells," *Solar Energy Materials & Solar Cells* 203 (2019): 110120.

9. H. J. Park, H. Park, S. J. Park, et al., "Passivation Quality Control in Poly-Si/SiO_x/c-Si Passivated Contact Solar Cells With 734 mV Implied Open Circuit Voltage," *Solar Energy Materials & Solar Cells* 189 (2019): 21–26, https://doi.org/10.1016/j.solmat.2018.09.013.

10. D. M. Chen, Y. F. Chen, Z. G. Wang, et al., "24.58% Total Area Efficiency of Screen-Printed, Large Area Industrial Silicon Solar Cells With the Tunnel Oxide Passivated Contacts (I-TOPCon) Design," *Solar Energy Materials and Solar Cells* 206 (2020): 110238.

11. M. A. Green, E. D. Dunlop, M. Yoshita, et al., "Solar Cell Efficiency Tables (Version 64)," *Progress in Photovoltaics: Research and Applications* 32 (2024): 425–441.

12. D. Pysch, A. Mette, A. Filipovic, and S. W. Glunz, "Comprehensive Analysis of Advanced Solar Cell Contacts Consisting of Printed Fine-Line Seed Layers Thickened by Silver Plating," *Progress in Photovoltaics: Research and Applications* 17, no. 2 (2009): 101–114.

13. A. Moldovan, F. Feldmann, M. Zimmer, J. Rentsch, J. Benick, and M. Hermle, "Tunnel Oxide Passivated Carrier-Selective Contacts Based on Ultra-Thin SiO_2 Layers," *Solar Energy Materials & Solar Cells* 142 (2015): 123–127.

14. Y. Larionova, M. Turcu, S. Reiter, et al., "On the Recombination Behavior of p^+-Type Polysilicon on Oxide Junctions Deposited by Different Methods on Textured and Planar Surfaces," *Physica Status Solidi A* 214, no. 8 (2017): 1700058.

15. K. R. Mclntosh and L. P. Johnson, "Recombination at Textured Silicon Surfaces Passivated With Silicon Dioxide," *Journal of Applied Physics* 105, no. 12 (2009): 40–78.

16. A. S. Kale, W. Nemeth, H. Guthrey, et al., "Modifications of Textured Silicon Surface Morphology and Its Effect on Poly-Si/SiO_x Contact Passivation for Silicon Solar Cells," *IEEE Journal of Photovoltaics* 9, no. 6 (2019): 1513–1521.

17. R. R. Razouk and B. E. Deal, "Dependence of Interface State Density on Silicon Thermal Oxidation Process Variables," *Journal of the Electrochemical Society* 126, no. 9 (1979): 1573–1581.

18. Y. Kato, H. Takao, K. Sawada, and M. Ishida, "Improvement of Metal-Oxide Semiconductor Interface Characteristics in Complementary Metal-Oxide Semiconductor on Si (111) by Combination of Fluorine Implantation and Long-Time Hydrogen Annealing," *Japanese Journal of Applied Physics* 45, no. 4 (2006): L108–L110.

19. H. Guthrey, C. L. Anderson, A. S. Kale, et al., "Effect of Surface Texture on Pinhole Formation in SiO_x-Based Passivated Contacts for High-Performance Silicon Solar Cells," *ACS Applied Materials & Interfaces* 12, no. 50 (2020): 55737–55745.

20. N. C. Mandal, S. Biswas, S. Acharya, et al., "Study of the Properties of SiO_x Layers Prepared by Different Techniques for Rear Side Passivation in TOPCon Solar Cells," *Materials Science in Semiconductor Processing* 119 (2020): 105163.

21. M. Fırat, M. R. Payo, F. Duerinckx, J.-M. Luchies, M. Lenes, J. Poortmans "Characterization of Absorption Losses in Rear Side N-Type Polycrystalline Silicon Passivating Contacts," 15th International Conference on Concentrator Photovoltaic Systems (CPV-15) (2019).

22. K. Tao, Q. Li, C. Hou, et al., "Application of A-Si/μc-Si Hybrid Layer in Tunnel Oxide Passivated Contact n-Type Silicon Solar Cells," *Solar Energy* 144 (2017): 735–739.

23. H. Han, D. Choi, S. Jeong, et al., "Effects of Surface Morphology on Ag Crystallite Formation in Screen-Printed Multi-Crystalline Si Solar Cells," *Materials Science in Semiconductor Processing* 128 (2021): 105759.

24. G. Kulushich, R. Z. Gottwick, V. X. Nguyen, and J. H. Werner, "Role of Phosphorus in Contact Formation on Silicon Solar Cells," *Physica Status Solidi Rapid Research Letters* 6, no. 9–10 (2012): 370–372.

25. E. Cabrera, S. Olibet, J. G. Reichenbach, R. Kopecek, and G. Schubert, "Experimental Evidence of Direct Contact Formation for the Current Transport in Silver Thick Film Metalized Silicon Emitters," *Journal of Applied Physics* 110, no. 11 (2011): 114511.

26. A. Chaudhary, J. Hoß, J. Lossen, et al., "Influence of Silicon Substrate Surface Finish on the Screen-Printed Silver Metallization of Polysilicon-Based Passivating Contacts," *Physica Status Solidi* 219, no. 9 (2022): 2100869, https://doi.org/10.1002/pssa.202100869.

27. M. Fırat, H. S. Radhakrishnan, M. R. Payo, F. Duerinckx, L. Tous, and J. Poortmans, "In Situ Phosphorus-Doped Polycrystalline Silicon Films by Low Pressure Chemical Vapor Deposition for Contact Passivation of Silicon Solar Cells," *Solar Energy* 231, no. 2022 (2022): 78–87.

28. R. A. Sinton and A. Cuevas, "Contactless Determination of Current-Voltage Characteristics and Minority-Carrier Lifetimes in Semiconductors From Quasi-Steady-State Photoconductance Data," *Applied Physics Letters* 69 (1996): 2510–2512.

29. D. E. Kane, R. M. Swanson. "Measurement of the Emitter Saturation Current by a Contactless Photoconductivity Decay Method," in: In 18th IEEE PVSC, las Vegas, (1985): 578–583. USA.

30. R. A. Sinton and R. M. Swanson, "Recombination in Highly Injected Silicon," *IEEE Transactions on Electron Devices* 34, no. 6 (1987): 1380–1389, https://doi.org/10.1109/T-ED.1987.23095.

31. Y. Kang, Q. Yu, Z. Lei, and H. Ming, "An Application of Raman Spectroscopy on the Measurement of Residual Stress in Porous Silicon," *Optics and Lasers in Engineering* 43 (2005): 847–855.

32. S. Ma, D. X. Du, D. Ding, et al., "Improving the Performance of Industrial TOPCon Solar Cells Through the Insertion of Intrinsic A-Si Layer," *Solar Energy Materials and Solar Cells* 275 (2024): 113024.

33. E. Anastassakis, A. Canterero, and M. Cardona, "Piezo-Raman Measurements and Anharmonic Parameters in Silicon and Diamond," *Physical Review B: Condensed Matter* 41 (1990): 7529–7535.

34. Y. R. Lin, Z. H. Yang, Z. K. Liu, et al., "Dual-Functional Carbon-Doped Polysilicon Films for Passivating Contact Solar Cells: Regulating Physical Contacts While Promoting Photoelectrical Properties," *Energy & Environmental Science* 14 (2021): 6406–6418.